Low-temperature thermoelectric power of CaB_6

2002 J. Phys.: Condens. Matter 14 1035

(http://iopscience.iop.org/0953-8984/14/5/308)

INSTITUTE OF PHYSICS PUBLISHING JOURNAL OF PHYSICS: CONDENSED MATTER

J. Phys.: Condens. Matter **14** (2002) 1035–1043 PII: S0953-8984(02)30290-X

Low-temperature thermoelectric power of CaB_6

K Giannò[1], A V Sologubenko[1], H R Ott[1], A D Bianchi[2] and Z Fisk[2]

[1] Laboratorium für Festkörperphysik, ETH Hönggerberg, CH-8093 Zürich, Switzerland
[2] National High Magnetic Field Laboratory, Florida State University, 1800 East Paul Dirac Drive, Tallahassee, FL 32306, USA

Received 26 October 2001
Published 25 January 2002
Online at stacks.iop.org/JPhysCM/14/1035

Abstract

We report the results of measurements of the thermoelectric power S of stoichiometric CaB_6 and vacancy-doped $Ca_{1-\delta}B_6$ between 5 and 300 K. The thermopower for both materials is surprisingly large at room temperature. Across the whole temperature range covered, S is negative and the temperature dependence is most probably dictated by band-structure effects. The phenomenological interpretation of our data involves a calculation of $S(T)$, using the Boltzmann equation in the relaxation time approximation and assuming a band of defect states in proximity to the lower edge of the conduction band. Good agreement with our data is found by considering acoustic phonon and ionized impurity scattering for the electrons in the conduction band, which is well separated from the valence band.

1. Introduction

Recent experiments on hexaborides with divalent metal cations of the alkaline-earth series, namely Ca, Sr, and Ba, have revealed some unusual physical properties of these materials. In particular, an itinerant type of weak ferromagnetic order, stable up to temperatures between 600 and 900 K, has been observed in CaB_6 and related alloys in a narrow range of electron doping [1–3]. The electronic properties of alkaline-earth hexaborides place these materials close to a metal–insulator transition [2, 4]. This has been supported theoretically by LDA calculations of the electronic structure of divalent hexaborides which indicate that, with the exception of a small region around the X point of the cubic Brillouin zone, the valence and the conduction bands are separated by a large gap of several electron volts [5]. The slight band overlap is reduced if the inter-octahedron B–B bond distances increase; this finally results in the opening of a gap over the entire momentum space. It has also been predicted that the transport properties of SrB_6 may be strongly dependent on doping, with changes from a p-type to an n-type metal induced by slight shifts of the Fermi energy around the zero-doping value [5]. These observations have led to the speculation that the ground state of undoped divalent hexaborides may be characterized by a Bose condensate of bound electron–hole pairs,

or excitons [6–8]. Weak ferromagnetism may then develop because of a spontaneous time-reversal symmetry breaking via doping. More recent GW-calculations of the single-particle excitation spectrum of CaB_6, however, have led to the claim that this material is not a semimetal but a semiconductor with a minimum band gap of 0.8 eV [9]. If this possibility is considered, the experimental observations, which suggest that binary hexaborides are close to a metal–insulator transition, would indicate the presence of a band of defect states for itinerant charge carriers.

Since the theoretical interpretation of the observed high-T_C ferromagnetism strongly depends on issues concerning the electronic band structure of these materials, additional information regarding the excitation spectrum of the electrons in CaB_6 is welcome. In an attempt to resolve the uncertainties with respect to the correct description of this material, the influence of the chemical composition on the physical properties of CaB_6 has been studied. The electrical resistivity, magnetoresistance, low-temperature specific heat, and optical conductivity of stoichiometric and doped CaB_6 samples have been investigated and the results have been presented in a previous publication [2]. Below, we present the results of measurements of the thermoelectric power S. While data on the electrical conductivity and the electronic contribution to the thermal conductivity provide information on the density of electronic states $N(E)$ close to the Fermi energy E_F, the thermopower may serve to establish the energy derivative of $N(E)$, i.e., an additional important detail of the electronic excitation spectrum. One of the samples was synthesized so as to obtain material with a close-to-stoichiometric composition, denoted as CaB_6. The second sample, which we denote as $Ca_{1-\delta}B_6$, contained a small number of vacancies on the calcium sites, inadvertently introduced during the flux-growth procedure and leading to a certain degree of self-doping which is difficult to control.

This paper is organized as follows: after a brief description of the sample preparation and the experimental methods used in this investigation in section 2, we present, in section 3, the results of our measurements and their analysis. The conclusions are presented in section 4.

2. Samples and experimental methods

Binary hexaborides can be synthesized in a narrow range of composition, with a claimed tendency to be boron rich with concentrations of metal vacancies up to several per cent. Stoichiometric CaB_6 crystals can be obtained close to the border of the metal-rich phase boundary [10]. For our experiments the single crystals were grown by a slow-cooling procedure in aluminium flux [11] starting with a nominal ratio CaB_3 for the stoichiometric CaB_6 sample, and with CaB_{12} for the metal-deficient $Ca_{1-\delta}B_6$ sample. The crystals were removed from the flux by leaching in a concentrated sodium hydroxide solution. Subsequent etching with HNO_3 was intended to remove possible surface contaminations. The samples on which our transport measurements were made were of prism-type shape with approximate overall dimensions of $4.2 \times 0.5 \times 0.45$ mm^3 for CaB_6 and $4.7 \times 0.45 \times 0.4$ mm^3 for $Ca_{1-\delta}B_6$.

The thermoelectric power S and the thermal conductivity κ of both samples were measured simultaneously by means of a standard steady-state heat-flow technique between 5 and 300 K. Since the thermal conductivity is dominated by lattice excitations, the results of these measurements will be presented elsewhere. A commercial ^{4}He-gas-flow cryostat was used for cooling the sample holder. At one end of the prism-shaped sample, the thermal contact to a copper heat sink was achieved by using high-conductance silver epoxy. The sample heater, consisting of a 100 Ω ruthenium oxide chip resistor, was attached to the other end of the prism by the same method. Joule heating caused by heater currents of the order of a few mA provided the necessary heat flow and hence a thermal gradient along the crystals. In order to

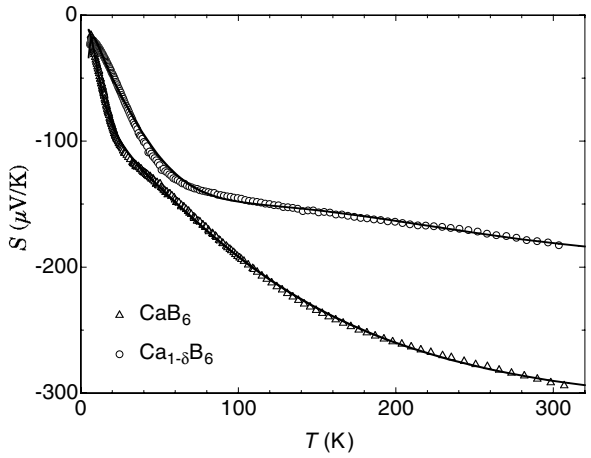

Figure 1. Temperature dependence of the thermoelectric power S, for CaB_6 and $Ca_{1-\delta}B_6$, on linear scales. The solid curves represent fits to our data, as explained in the text.

measure both the temperature difference ΔT between two contacts mounted perpendicularly to the heat flow and the thermoelectric voltage of our samples with respect to chromel, we used two pairs of calibrated 0.025 mm Au–Fe (0.07 at.%) versus chromel thermocouples [12]. The length of the thermocouples (10 cm) was chosen in order to reduce the heat losses through this channel to a negligible amount. The reliability of our experimental data measured in this way has been demonstrated in a previous publication [13], where the thermal gradient along the sample was measured by using both chromel–gold/iron thermocouples as well as calibrated carbon resistor thermometers in the temperature range around 2 K. In order to minimize spurious thermal voltages, the thermocouple leads were connected to uninterrupted copper wires reaching three home-built low-noise voltage amplifiers, mounted directly on top of the cryostat insert.

3. Experimental results and analysis

The thermoelectric power $S(T)$ for both samples is shown in figure 1 on linear scales. The negative sign of S clearly demonstrates the dominant n-type character of the crystals investigated. The rather large values of S, if compared to typical values observed for the thermoelectric power of common metals, are an indication for the low itinerant charge-carrier concentration in these materials, compatible with the very low values of the electrical conductivity reported previously [2]. The overall temperature dependence of S is obviously non-linear, with features that are reminiscent of band-structure effects affecting the temperature-induced variation of the thermopower of elements and crystalline alloys [14]. Nevertheless, below $T^* = 20$ and 40 K for CaB_6 and $Ca_{1-\delta}B_6$, respectively, the curves exhibit an approximately linear temperature dependence. A negative thermoelectric power varying linearly with T is usually identified as the diffusion thermopower S of metals, where the Fermi energy E_F is located within the conduction band. In the free-electron approximation,

$$S = -\frac{\pi^2 k_B^2 T}{3|e|E_F/s} \tag{1}$$

with E_F the Fermi energy measured from the bottom of the conduction band and s a factor, typically of the order of unity, describing the energy dependence of the scattering time

$\tau \propto E^{s-3/2}$ for the scattering mechanism dominating the low-temperature behaviour [14]. From the average slope of $S(T)$ below T^*, we may thus calculate a rescaled Fermi energy E_F/s. These values are $E_F/s = 4.5$ and 8.7 meV for CaB_6 and $Ca_{1-\delta}B_6$, respectively. Consideration of the entire temperature dependence of S, in particular the abrupt slope changes of $S(T)$ around T^*, suggests that ultimately $S(T)$ cannot be explained by simply taking into account electronic states in the conduction band alone. In the following, we try to identify the possible reasons for the measured departure from linearity in the temperature dependence of S.

With the common assumption that the current densities $\boldsymbol{j}$ and $\boldsymbol{w}$ for electrical and thermal transport, respectively, respond linearly to their driving forces, we can write

$$\begin{aligned} \boldsymbol{j} &= e^2 L_0 \boldsymbol{E} - \frac{e}{T} L_1 \boldsymbol{\nabla}_r T \\ \boldsymbol{w} &= e L_1 \boldsymbol{E} - \frac{1}{T} L_2 \boldsymbol{\nabla}_r T \end{aligned} \tag{2}$$

where $\boldsymbol{E}$ is the external electric field and $\boldsymbol{\nabla}_r T$ is the temperature gradient. In equation (2), the transport coefficients L_i ($i = 0, 1, 2$) explicitly fulfil the Onsager relations [15]. For $\boldsymbol{j} = 0$, we obtain $\boldsymbol{w} = -\kappa_{el} \boldsymbol{\nabla}_r T$ and $\boldsymbol{E} = S \boldsymbol{\nabla}_r T$, whereas for $\boldsymbol{\nabla}_r T = 0$, we get $\boldsymbol{j} = \sigma \boldsymbol{E}$. These are the equations defining the electronic contribution to the thermal conductivity κ_{el}, the thermoelectric power S, and the electrical conductivity σ, such that

$$\kappa_{el} = \frac{1}{T}\left(L_2 - \frac{L_1^2}{L_0}\right) \tag{3a}$$

$$S = -\frac{1}{|e|T}\frac{L_1}{L_0} \tag{3b}$$

$$\sigma = e^2 L_0. \tag{3c}$$

The integrals L_i ($i = 0, 1, 2$) are defined as

$$L_i = -\int_{-\infty}^{+\infty} \tilde{\sigma}(E)(E - E_F)^i \frac{\partial f_0}{\partial E}\, \mathrm{d}E \tag{4}$$

with $\tilde{\sigma}(E)$ representing the conductivity spectrum, including all system-dependent features. By partial integration of equation (4) and by using the Sommerfeld expansion scheme, we get

$$S = -\frac{\pi^2 k_B^2 T}{3|e|}\left(\frac{\partial \ln \tilde{\sigma}(E)}{\partial E}\right)_{E=E_F} \tag{5}$$

which approximates equation (3*b*) very well at temperatures $k_B T \ll E_F$. Since we intend to interpret our data over the entire temperature range covered and in view of the low values of E_F, we will not use the low-temperature approximation represented by equation (5) in our analysis. For our purposes the general form of S shown in equation (3*b*) is more appropriate.

Since $\tilde{\sigma}(E) > 0$, the coefficient L_0 is strictly positive and the sign of S is determined by the sign of the integral L_1. From inspecting the integrand of L_1, represented in equation (4), and also considering equation (3*b*), it may be concluded that the states with energies higher than the chemical potential, i.e., $E > E_F$, provide a negative contribution to the thermoelectric power, whereas those states which are located below E_F contribute with the opposite sign. At low temperatures, where only the states very close to E_F contribute to the electronic transport, the measured S-values are negative. This leads us to conclude that $\tilde{\sigma}(E)$ must increase monotonically across E_F, so the states contributing negatively to $S(T)$ in L_1 acquire a larger weight than those located below the Fermi energy, which contribute positively to $S(T)$. In order to reproduce the observed reduction of the slope of $S(T)$ at T^* in the calculation, however, we are forced to introduce a 'feature' in $\tilde{\sigma}(E)$ centred at an energy E^* such that $|E^* - E_F| \sim k_B T^*$. Since the absolute value of $\partial S/\partial T$ decreases

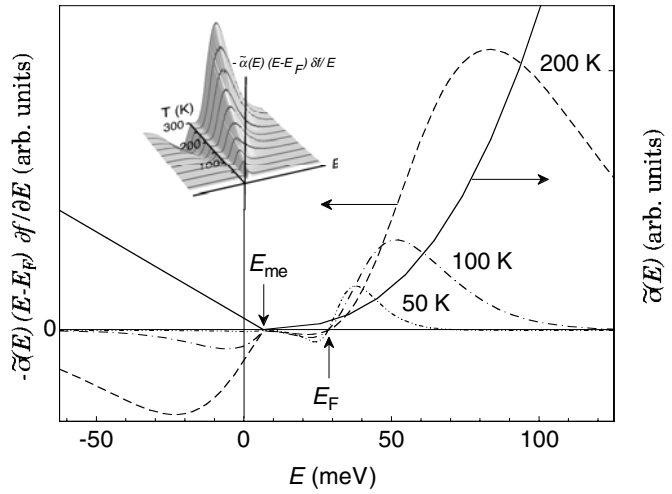

Figure 2. Auxiliary quantities, relevant in our analysis of $S(T)$. The solid curve is the postulated conductivity spectrum $\tilde{\sigma}(E)$ for $Ca_{1-\delta}B_6$. The various broken curves represent the value of the integrand appearing in L_1 as a function of energy for $T = 50, 100, 200$ K, as explained in the text. In the inset, the integrand of L_1 is shown as a function of T and E. For a given temperature, the thermoelectric power S is proportional to the integral taken along the curves shown on the three-dimensional surface.

above T^*, the feature in $\tilde{\sigma}(E)$ must either reduce the negative contribution to $S(T)$ given by the states above E_F, or else enhance the positive contribution to $S(T)$ of the states below E_F.

In what follows, we assume that in our case the second possibility is realized and we add an additional part to the $\tilde{\sigma}(E)$ spectrum, decreasing linearly with increasing energy below E_F. As an example, the complete chosen $\tilde{\sigma}(E)$ spectrum for $Ca_{1-\delta}B_6$, corresponding to the equations (7) and (10) below, is shown as the solid curve in figure 2.

On the basis of this preliminary analysis and the model outlined above, we have calculated the electronic transport properties of CaB_6 and $Ca_{1-\delta}B_6$. The Fermi energy is fixed within a parabolic conduction band. Close to the bottom of this band we position an additional band, which may be interpreted as a band of defect states. This scenario is supported by recent calculations of the electronic structure of point defects in CaB_6, suggesting that the non-zero charge-carrier concentration in the conduction band at $T = 0$ K is due to resonances arising from the presence of B and B_6 vacancies in the system [16]. With these assumptions, the conductivity spectrum may be written as

$$\tilde{\sigma}(E) = \tilde{\sigma}^{\mathrm{n}}(E) + \tilde{\sigma}^{\mathrm{p}}(E). \tag{6}$$

For an isotropic parabolic conduction band, the Boltzmann equation in the relaxation time approximation leads to

$$\tilde{\sigma}^{n}(E) = \begin{cases} 0 & (E < E_n) \\ \dfrac{1}{3\pi^2 m_n}\tau(E)\left(\dfrac{2m_n}{\hbar^2}\right)^{3/2}(E - E_n)^{3/2} & (E > E_n) \end{cases} \tag{7}$$

where the bottom of the conduction band has been fixed at $E_n = 0$ meV. Setting $\tilde{\sigma}(E) = \tilde{\sigma}^{n}(E)$ in equation (5), it is easy to recover equation (1). For the effective mass of the conduction electrons we used $m_n = 0.28m_0$ [5,9], with m_0 as the free-electron mass. We only considered

two scattering mechanisms of the charge carriers in the conduction band, i.e., scattering by acoustic lattice vibrations, approximated by a rate [17, 18]

$$\tau_{\mathrm{lv}}^{-1} = \alpha E^{1/2} T \tag{8}$$

and scattering by ionized impurities with a rate [18]

$$\tau_{\mathrm{ii}}^{-1} = \beta E^{-3/2} \tag{9}$$

where α and β are two constants to be determined by the fitting procedure. If the defect states which are forming a band below the bottom of the conduction band coexist with localized states, the latter may act, when ionized, as scattering centres for the electrons. This justifies considering a term τ_{ii}^{-1} in the scattering rate of the electrons. Another possibility is to attribute the rate τ_{ii}^{-1} to the vacancies at the Ca^{2+}-ion sites which would act as negatively charged scattering centres. With the common assumption that the two scattering mechanisms do not interfere with each other, we may use Matthiessen's rule in the form $\tau = (\tau_{\mathrm{lv}}^{-1} + \tau_{\mathrm{ii}}^{-1})^{-1}$ for the electrons' average scattering time.

For the defect band, we postulate [19]

$$\tilde{\sigma}^{p}(E) = \begin{cases} \gamma(E_{\mathrm{me}} - E) & (E < E_{\mathrm{me}}) \\ 0 & (E > E_{\mathrm{me}}) \end{cases} \tag{10}$$

with a mobility edge E_{me} and γ a constant. Since the quantities L_0 and L_1 which dictate the temperature dependence of the thermopower appear in the ratio L_1/L_0, S depends only on the relative magnitude of the constants α, β and γ. This allows some reduction of the number of fitting parameters. In figure 1, the solid curves represent the results of the calculation of $S(T)$. Considering the simplicity of the model and the small number of free parameters (α/γ, β/γ, E_{F}, and E_{me}), the agreement with the experimental data is quite remarkable. The Fermi energies which emerge from the fitting procedure amount to 14 and 28 meV for CaB_6 and $Ca_{1-\delta}B_6$, respectively, corresponding to 0 K charge-carrier densities n_{c} of 1.1×10^{24} m^{-3} and 3.2×10^{24} m^{-3}, or to 0.8×10^{-4} and 2.3×10^{-4} charge carriers per unit cell, respectively. Preliminary results [20] of low-temperature Hall effect measurements performed on a CaB_6 sample with the same resistivity as our vacancy-doped sample lead, when interpreted with a single-band model, to a charge-carrier density of 4.2×10^{24} m^{-3}, and are hence compatible with our results. The value of the mobility edge E_{me}, introduced to reproduce the kink in $S(T)$ at the observed temperatures, is approximately +8 meV for both samples. We note, however, that this value strongly depends on the choice of the energy exponent of the low-temperature scattering term. We have to admit that, in this sense, the result depends on the model employed.

Our calculation of the thermoelectric power relies essentially on the model of the conductivity spectrum (modulo a factor), which we may now test by calculating other electronic transport properties such as the electrical resistivity $\rho(T)$ and comparing the results with experimental data. In figure 3, we have plotted the rescaled electrical resistivity of CaB_6 calculated with equation (3*c*), together with the experimental data obtained on two samples of the same batch. We emphasize here that the continuous line *is not* a fit to experimental results but a consequence of our description of the thermoelectric power by using a two-band model as described above. The temperature dependence of the calculated $\rho(T)$ reproduces, at least qualitatively, the salient temperature-dependent features of the experimental data. Our calculations show that the rapid decrease of $\rho(T)$ above 100 K may be obtained by activating the electrons which are residing in a defect band located at the edge of the conduction band. It seems difficult to reconcile our data with the excitonic scenario [6–8] which has been suggested to explain the high-T_{C} ferromagnetism in these materials.

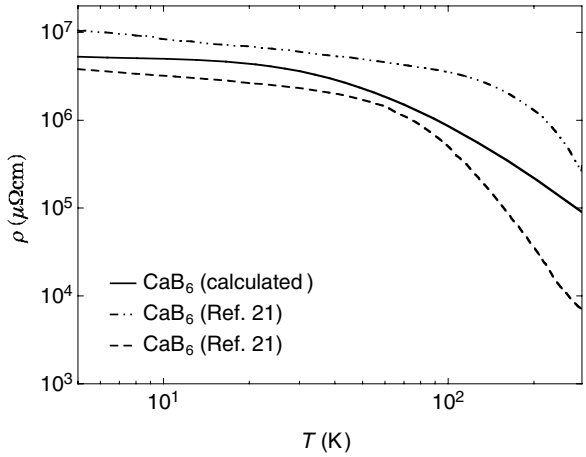

Figure 3. The solid curve represents the expected temperature dependence of the electrical resistivity of CaB_6 which is based on the postulated conductivity spectrum $\tilde{\sigma}(E)$, as explained in the text. Also shown in the figure as dash–dotted and broken curves are the measured temperature dependencies of the resistivities of two samples [21] originating from the same batch as the CaB_6 sample measured in this investigation.

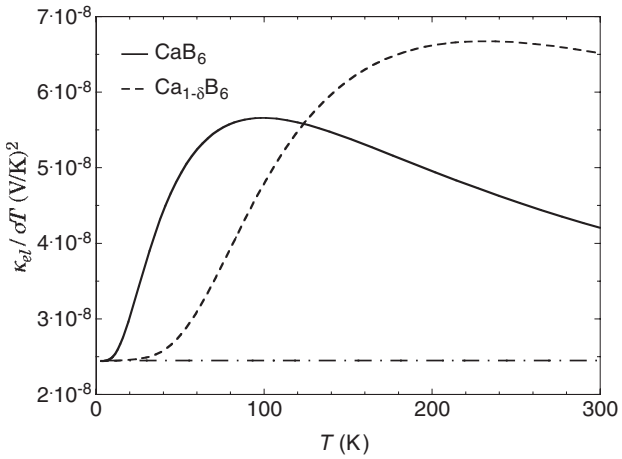

Figure 4. The ratio $\kappa_{\rm el}/\sigma T$ as a function of temperature, calculated by using equations (3*a*) and (3*c*), and the fit parameters resulting from our analysis of $S(T)$ for CaB_6 (solid curve) and $Ca_{1-\delta}B_6$ (dashed curve). The horizontal dashed–dotted curve represents the temperature-independent Lorenz number $\tilde{L}_0 = 2.45 \times 10^{-8}$ V^2 K^{-2}.

By using equations (3*c*), (4), and (7), combined with the measured resistivity curves shown in figure 3, we conclude that the mean free path $l_{\rm F} = \hbar k_{\rm F} \tau(E_{\rm F})/m_n$ of the conduction electrons in CaB_6 is less than 100 Å. The same length is obtained, obviously, by employing the Drude formula $\sigma = ne^2\tau/m_n$ and by using $n = n_{\rm c}$, the value cited above for the charge-carrier concentration of CaB_6. Since the electrons' wavevector at the Fermi energy is of the order of 10^{-2} Å^{-1}, it seems reasonable to assume that the Ioffe–Regel criterion for localization ($k_{\rm F} l_{\rm F} < 1$) is close to being fulfilled in CaB_6.

A measure for the electronic contribution to the thermal conductivity is given by the quantity $L^* = \kappa_{el}/\sigma T$, which can be calculated from equations (3*a*) and (3*c*). Just like the thermoelectric power S, L^* depends only on the relative magnitude of the constants α, β, and γ. In a degenerate one-band model, the value

$$\kappa_{el}/\sigma T = \tilde{L}_0 = \frac{\pi^2}{3}\left(\frac{k_B}{e}\right)^2 \tag{11}$$

is denoted as the *Lorenz number*. In figure 4 we plot the temperature dependence of L^*, calculated from the fitting parameters provided by our analysis of $S(T)$, together with the value $\tilde{L}_0 = 2.45 \times 10^{-8}\ V^2\ K^{-2}$. As expected, $\kappa_{el}/\sigma T$ is equal to the Lorenz number at very low temperatures. This is so because only the electrons of the conduction band contribute to the transport. The value L^* becomes larger than $\tilde{L}_0$ at those temperatures at which the impurity states start to contribute to κ_{el}. At the warm end of the crystal, more defect states are excited across the Fermi energy than at the cold end, where additional quasiparticles release their excitation energy. It will be demonstrated in a separate publication that despite the enhancement of L^*, the contribution of the electrons to the measured thermal conductivity is negligible.

4. Summary and conclusions

We have measured the thermoelectric power of close-to-stoichiometric and vacancy-doped CaB_6 between 5 and 300 K. The high negative values of the thermoelectric power $S(T)$ for both materials indicate a low concentration of itinerant n-type charge carriers. We have achieved a reasonable interpretation of $S(T)$ by using a relaxation time approximation of Boltzmann's equation, by considering a sizable gap between valence and conduction band states, and by postulating the existence of an additional term in the conductivity spectrum which may be related to the existence of a band of defect states in proximity to the lower edge of the conduction band.

Acknowledgments

We thank R Monnier and M E Zhitomirsky for stimulating discussions. This work was financially supported by the Schweizerische Nationalfonds zur Förderung der Wissenschaftlichen Forschung.

References

[1] Young D P, Hall D, Torelli M E, Fisk Z, Sarrao J L, Thomson J D, Ott H R, Oseroff S B, Goodrich R G and Zysler R 1999 *Nature* **397** 412
[2] Vonlanthen P, Felder E, Degiorgi L, Ott H R, Young D P, Bianchi A D and Fisk Z 2000 *Phys. Rev.* B **62** 10 076
[3] Ott H R, Gavilano J L, Ambrosini B, Vonlanthen P, Felder E, Degiorgi L, Young D P, Fisk Z and Zysler R 2000 *Physica* B **281+282** 423
[4] Ott H R, Chernikov M, Felder E, Degiorgi L, Moshopoulou E G, Sarrao J L and Fisk Z 1997 *Z. Phys.* B **102** 337
[5] Massidda S, Continenza A, de Pascale T M and Monnier R 1997 *Z. Phys.* B **102** 83
[6] Zhitomirsky M E, Rice T M and Anisimov V I 1999 *Nature* **402** 251
[7] Balents L and Varma C M 2000 *Phys. Rev. Lett.* **84** 1264
[8] Barzykin V and Gor'kov L P 2000 *Phys. Rev. Lett.* **84** 2207
[9] Tromp H J, van Gelderen P, Kelly P J, Brocks G and Bobbert P A 2000 *Phys. Rev. Lett.* **87** 016401
[10] Spear K E 1977 *Boron and Refractory Borides* (Berlin: Springer) p 442
[11] Fisk Z and Remeika J P 1989 Growth of single crystals from molten metal fluxes *Handbook on the Physics and Chemistry of Rare Earths* vol 12, ed K A Gschneidner and L Eyring (New York: Elsevier) pp 53–71

[12] Bougrine H and Ausloos M 1995 *Rev. Sci. Instrum.* **66** 199
[13] Giannò K, Sologubenko A V, Chernikov M A, Ott H R, Fisher I R and Canfield P C 2000 *Phys. Rev.* B **62** 292
[14] Barnard R D 1972 *Thermoelectricity in Metals and Alloys* (London: Taylor and Francis)
[15] Blatt F J and Schroeder P A 1978 *Thermoelectricity in Metallic Conductors* (New York: Plenum) p 7
[16] Monnier R and Delley B 2001 *Phys. Rev. Lett.* **87** 157204
[17] Ziman J M 1960 *Electrons and Phonons* (London: Oxford University Press) pp 310–433
[18] Nag B R 1972 *Theory of Electrical Transport in Semiconductors* (Oxford: Pergamon) pp 105–115
[19] Enderby J E and Barnes A C 1994 *Phys. Rev.* B **49** 5062
[20] Wälti C 2001 private communication
[21] Bianchi A D 2001 private communication